Distribution Agreement

In presenting this thesis as a partial fulfillment of the requirements for a degree from Emory University, I hereby grant to Emory University and its agents the non-exclusive license to archive, make accessible, and display my thesis in whole or in part in all forms of media, now or hereafter now, including display on the World Wide Web. I understand that I may select some access restrictions as part of the online submission of this thesis. I retain all ownership rights to the copyright of the thesis. I also retain the right to use in future works (such as articles or books) all or part of this thesis.

Su Hyun Kim December 5, 2023

Applying an Automated Radiation Therapy Volume Analysis Pipeline to Determine the Utility of Spectroscopic MRI-guided Adaptive Radiation Therapy for Glioblastoma

by

Su Hyun (Senna) Kim

Hyunsuk Shim
Adviser

Quantitative Science

Hyunsuk Shim

Adviser

Weihua An

Committee Member

Phillip Wolff

Committee Member

2023

Applying an Automated Radiation Therapy Volume Analysis Pipeline to Determine the Utility of Spectroscopic MRI-guided Adaptive Radiation Therapy for Glioblastoma

By

Su Hyun (Senna) Kim

Hyunsuk Shim

Adviser

An abstract of
a thesis submitted to the Faculty of Emory College of Arts and Sciences
of Emory University in partial fulfillment
of the requirements of the degree of
Bachelor of Science with Honors

Quantitative Science

2023

Abstract

Applying an Automated Radiation Therapy Volume Analysis Pipeline to Determine the Utility of Spectroscopic MRI-guided Adaptive Radiation Therapy for Glioblastoma
By Su Hyun Kim

Due to the infiltrative nature of glioblastoma, tumor characterization is often inadequate with clinical imaging alone, resulting in suboptimal radiation therapy (RT) targeting. Precise targeting by whole-brain spectroscopic MRI (sMRI), which maps tumors using metabolites including choline (Cho) and N-acetylaspartate (NAA), can quantify early treatment-induced molecular changes that other modalities cannot measure. We have developed a pipeline to determine the degree of sMRI changes during early stages of RT and its association with patient outcomes. Such information can provide insight into the potential utility of adaptive RT (ART).

Data was obtained from a study (NCT03137888) where glioblastoma patients received high-dose RT guided by the pre-RT Cho/NAA twice normal (Cho/NAA ≥ 2x) volume, and received spectroscopic MRI scans pre- and mid-RT. After co-registering pre- and mid-RT Cho/NAA ≥2 volumes, spatial overlap statistics between the volumes for each patient (n=27) were calculated to quantify metabolic activity changes after two weeks of RT. Overall and progression-free survival (OS/PFS) Kaplan-Meier curves were generated, stratified by the median statistic begin plotted, and Log-rank tests were used to quantify the relationships between imaging metrics and OS/PFS.

Between the pre- and mid-RT Cho/NAA ≥ 2x volumes of all 27 patients, the median total overlap was 0.796 (range: 0 – 0.964), median Jaccard coefficient was 0.224 (0 – 0.723), median Dice coefficient was 0.365 (0 – 0.839), median volume similarity was -0.142 (-1.54 – 1.77), and median Hausdorff distance was 20.8 mm (8.54 – 92.2 mm). Patients with lower Jaccard/Dice coefficients had longer PFS (p=0.045 for both), and patients with lower Jaccard/Dice coefficients had higher OS trending towards significance (p=0.060 for both). Cho/NAA ≥ 2x volumes changed significantly during early RT, putting healthy tissue at risk of irradiation, and warranting further study into using adaptive RT planning.

Applying an Automated Radiation Therapy Volume Analysis Pipeline to Determine the Utility of Spectroscopic MRI-guided Adaptive Radiation Therapy for Glioblastoma

By

Su Hyun (Senna) Kim

Hyunsuk Shim

Adviser

A thesis submitted to the Faculty of Emory College of Arts and Sciences
of Emory University in partial fulfillment
of the requirements of the degree of
Bachelor of Science with Honors

Quantitative Science

2023

Table of Contents

1. Introduction

Glioblastoma is an aggressive brain cancer and is the most common primary brain malignancy [1,2]. Despite aggressive standard of care treatment for glioblastomas, the median survival is 15-16 months with frequent recurrence within 4-6 months [3]. One of the challenges that arises during glioblastoma treatment is precisely defining the radiation therapy (RT) target. Conventional imaging involves T1-weighted contrast enhanced (T1w-CE) MRI and T2-weighted fluid-attenuated inversion recovery (FLAIR) MRI. T1w-CE identifies glioblastoma by a gadolinium-based contrast agent but fails to identify non-enhancing infiltrative tumor regions. FLAIR is not specific to tumor in that it identifies abnormalities including edema, inflammation, and radiation effects [4-6]. Standard of care RT typically involves treating the resection cavity and the residual contrast enhancement on the T1w-CE MRI to a dose of 60 Gy and treating FLAIR hyperintensity to a dose of 45 – 54 Gy, followed by adjuvant temozolomide [3,7]. In a standard of care treatment course, the dosage and the treatment volumes are determined when the treatment is initiated, and are not altered during the course of treatment. However, for treating glioblastomas, the combination of T1w-CE and FLAIR MRIs to identify the RT target may not sufficiently identify infiltrative tumor and can thus result in undertreatment.

Combined with clinical imaging, magnetic resonance spectroscopy (MRS) measures metabolic concentrations that can identify infiltrative tumor without the use of contrast agents. An advanced form of MRS imaging, termed spectroscopic MRI, is a 3D whole-brain magnetic resonance spectroscopic imaging technique that identifies infiltrative,

non-enhancing tumor with high specificity [8-11]. For glioblastoma, two metabolites of interest include choline (Cho) and N-acetylaspartate (NAA). Compared to healthy tissue, Cho levels are elevated in tumor tissue due to increased membrane synthesis in proliferating cells, and NAA levels are decreased due to loss of healthy neuronal function. Image-histology correlation studies have shown that the Cho/NAA ratio is a highly specific tumor biomarker [12].

Changes in metabolically abnormal regions throughout the course of radiation therapy may be useful to provide insight into response to treatment. To monitor volumetric changes, we have developed a pipeline that quantifies the change in treatment volumes during treatment and analyzes how this change is related to patient outcomes. In this report, we show the results of using our tool on a cohort of patients enrolled in a recently completed multisite clinical study (NCT03137888).

Information about volumetric changes in metabolic abnormality during treatment can provide insight into the potential utility of adaptive RT planning, a method not commonly used in glioblastoma treatment [13-17]. Adaptive RT planning is a strategy which modifies the radiation plan to accommodate changes in tumor and brain morphology during treatment to maximize the benefit of radiation fractions later in the therapy course [13]. The process involves modifying dose, field margin, field shape, and beam intensity according to variations in the treatment target during the early stages of RT. A key component to adaptive RT is the use of an imaging modality that can detect changes due to treatment early on. Since spectroscopic MRI directly images metabolic changes, it is ideally suited for this task compared to conventional imaging. The

application of our pipeline in this context will attempt to demonstrate the outcome prediction capability of spectroscopic MRI after two weeks of treatment (during week 3), determining the potential utility of using this modality to guide adaptive RT planning.

2. Materials and Methods

To perform analysis of clinical and spectroscopic MRIs, we have developed a quantitative tool that can provide volumetric and statistical comparisons of different RT volumes and metabolite maps. It is fully implemented in Python, primarily using pydicom and SimpleITK for reading DICOM files and performing image registration, lifelines for all statistical analysis, NumPy for all basic image operations, and matplotlib and The Visual Toolkit (VTK) for visualization [18-21].

2.1. Data Acquisition and RT Planning

The data used in this study were acquired as part of our multisite pilot study (NCT03137888) in which 30 newly diagnosed WHO grade IV glioblastoma patients were treated to an escalated dose of 75 Gy guided by metabolic abnormality identified on spectroscopic MRI. Details regarding enrollment and initial survival outcomes have been previously reported [22]. In this study, data from one patient was unavailable. Additionally, two patients had IDH mutations, which is no longer considered to be glioblastoma as of 2021 [23]. As a result, 27 patients were used for the analysis presented in this report. Of these 27 patients, 7 were MGMT promoter hypermethylated.

Approximately 3-4 weeks after resection and one week prior to starting RT (pre-RT), clinical (T1w-CE and FLAIR) and spectroscopic MRIs were acquired. After each patient had completed two weeks of RT (mid-RT), spectroscopic, pre-contrast T1, and FLAIR MRIs were acquired. Post-contrast T1 MRIs were not acquired at mid-RT to avoid the cost and risk of an additional contrast injection. All scans were processed and registered to T1 MRIs for each patient. At each site, spectroscopic MRIs were acquired on a Siemens 3T scanner with GRAPPA-accelerated echo planar spectroscopic imaging. A 20- or 32-channel head and neck coil was used, and the data was acquired with 50 ms echo time (TE), 1551 ms repetition time (TR), and 71° flip angle [22]. Raw MRS data in DICOM files were processed using MIDAS software suite (University of Miami, Miami, FL, USA). MIDAS contains an automated MRSI processing pipeline, which includes lipid artifact removal by k-space extrapolation, fitting spectral analysis for metabolites of interest that are NAA, creatine, choline, signal normalization based on tissue water signal [27]. This pipeline eventually outputs 3D whole brain metabolite maps. These maps are then imported to Brain Imaging Collaboration Suite (BrICS), in which metabolite heat maps are visualized for RT planning.

2.2. RT Planning

Pre- and mid-RT Cho/NAA abnormal volumes were created by contouring regions greater than or equal to two times the average Cho/NAA (Cho/NAA ≥ 2x) value in normal appearing white matter that is contralateral to the tumor. Volumes were generated automatically in BrICS from each patients' spectroscopic MRI scans acquired

pre- and mid-RT [24]. Both contours were manually edited and checked by MRS experts based on spectral quality [24]. The pre-RT anatomic image used for registration was the T1w-CE, and the mid-RT anatomic image used the pre-contrast T1, since T1w-CE was not collected mid-RT. To perform the analysis depicted in Figure 1, the Cho/NAA ≥ 2x contours and the corresponding T1s and metabolite maps are inputted to the pipeline after being exported from BrICS as a series of DICOM files.

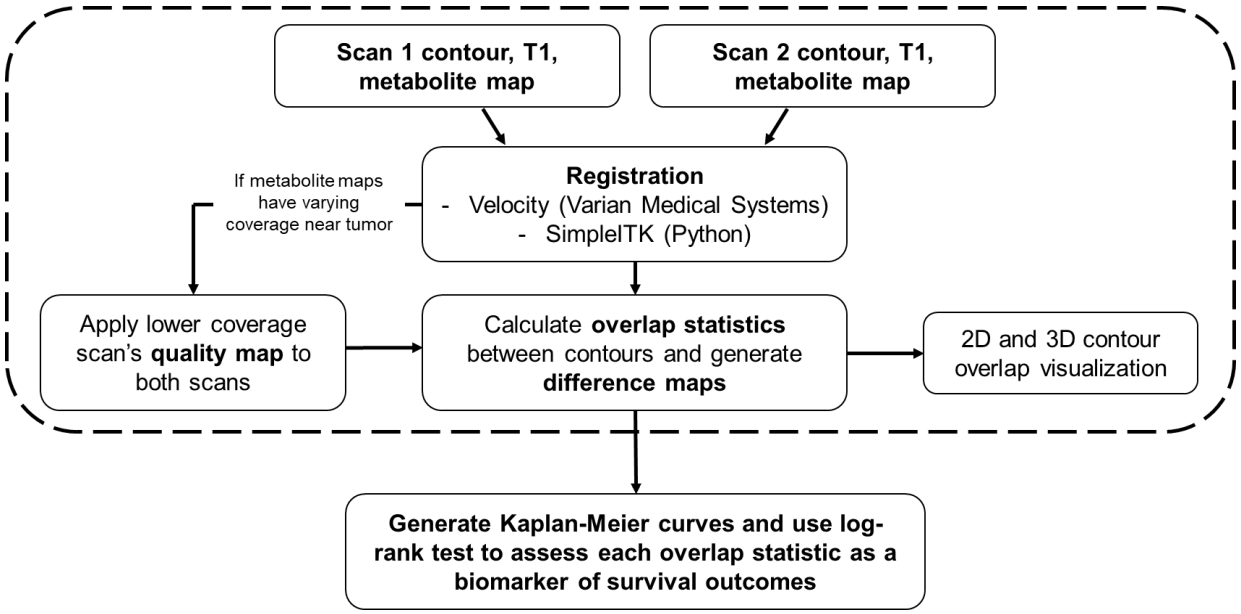

Figure 1. A flowchart detailing every component of the pipeline described in this report. The user first inputs a pair of contours, T1s, and metabolite maps. All images from the second scan are registered to the first scan either in Velocity (Varian Medical Systems) or within the program using SimpleITK. After approval of registration, if metabolite maps have varying coverage in the vicinity around the tumor, then the quality map for the lower coverage scan is applied to both scans to maintain coverage across both metabolite maps. Overlap statistics between the two contours are then calculated, and difference maps are generated for each axial slice based on the new,

modified metabolite maps. After this step, 2D and 3D renderings of the contours can be generated. The steps within the dashed box must be repeated for each pair of contours within a cohort of patients. The final step is to generate Kaplan-Meier curves for OS and PFS for each overlap statistic, stratifying the groups by the median value of the statistic of interest. A log-rank test is performed on each pair of Kaplan-Meier curves to determine if the overlap statistic used is a statistically significant biomarker of survival.

The pre-RT volume combined with the residual contrast enhancement from the T1w-CE received an escalated dose of 75 Gy, while the FLAIR abnormal regions received 50.1 Gy and the resection cavity received 60 Gy. More details regarding patient treatment have been previously reported [22]. Upon completing RT, follow-up imaging acquired every 2-3 months was used to determine PFS [25]. OS was determined based on communication with the patients and their oncology team as well as chart review.

2.3. Registration

Rigid and/or deformable registration was performed either using the Velocity software (Varian Medical Systems) or our SimpleITK registration implemented in Python. Both Velocity and our implementation have options to perform linear registration and deformable registration. Registration can be checked visually with a blend of the two images. Depending on the time between scans and degree of morphology change, linear registration may be sufficient. In order to proceed with the automatic analysis, every subject's registration must be approved by the user, after which the second scan is re-sampled with the registration transform applied and saved.

The T1 from the mid-RT scan was first registered to the T1w-CE from the pre-RT scan. Once approved, the transformation was applied to all remaining data (contours and metabolite maps) associated with the mid-RT scan. All results were carefully inspected by two authors (A.G.T. and S.K.) and approved by the board-certified medical physicist (E.S.) who is specialized in image registration. The registered images were resampled and then stored in addition to the original images and were used for all remaining analyses.

2.4. Metabolite Map Coverage

For spectroscopic MRI maps, during initial data processing, poor quality spectra were removed based on various criteria [26-31]. Voxels with a metabolite linewidth greater than 18 Hz were removed due to poor quality as an initial filtering step. This process generates a quality map, which is a mask that identifies the voxels that passed all criteria. For data acquired during this trial, the brain coverage was 70-75% after automatic artifact filtration to remove poor quality spectra.

Such filtering may result in differences in coverage between two scans of a patient in areas surrounding tumor. To allow for an unbiased comparative analysis, the quality maps of pre- and mid-RT scans of each patient were applied to one another to only include voxels that passed all spectra quality criteria in both scans. This was achieved by exporting each quality map as a binary NumPy array, then applying pre- and mid-RT quality maps to one another for each patient. This process created a lower coverage

mask for each patient, which was then applied to the metabolite maps and contours generated based on metabolic abnormality for both scans.

2.5. Overlap Statistics

To quantify volumetric differences in contours, we calculate a variety of spatial overlap statistics [32]. For binary mask contours *A* (earlier scan) and *B* (later scan), total overlap is calculated by identifying the number of pixels in the intersection of *A* and *B* divided by the number of pixels in *B*. Jaccard coefficient (union overlap) is two times the number of pixels in the intersection of *A* and *B* divided by the number of pixels in the union of *A* and *B*. Dice coefficient (mean overlap) is two times the number of pixels in the intersection of *A* and *B* divided by the sum of the total pixels in *A* and the total pixels in *B*. The final metric calculated is Hausdorff distance, which represents the maximum distance of *A* to the nearest point in *B* [33]. The final quantities calculated are the direction and percentage of volume change. Neither quantity takes any spatial information into account, they only consider the change in volume. Volume change is calculated by taking the absolute value of the difference between the volume of *A* and *B* divided by volume of *A*. Direction information is preserved by not taking the absolute value of the volume differences.

2.6. Visualization

To visually validate the results of the overlap statistics, 2D and 3D visualizations of the inputted contours and metabolite maps are generated. 2D visualization involves overlaying the contour on top of the corresponding T1 and metabolite map, and 3D visualization renders the two contours on the same plane so that differences in the contours can be identified. Additionally, the difference between normalized maps can be visualized, and are saved as 3D NumPy arrays. An example of 2D and 3D visualization, including a difference map, is shown in Figure 2. When running the 3D visualization code, contours can be rotated and zoomed in/out as well as altered in their opacity. A demonstration of the interactive 3D visualization is available in the online Supplemental Video 1.

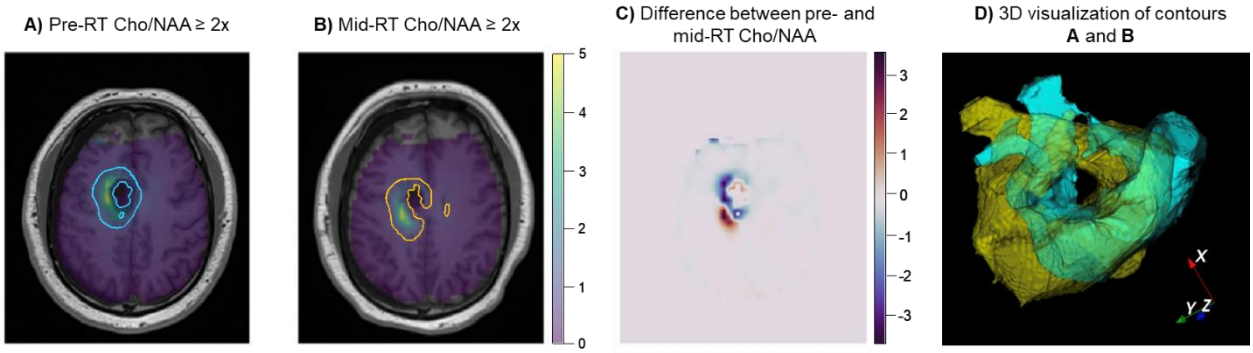

Figure 2. An example of the 2D and 3D visualization generated by the pipeline for a given subject. A and B show the pair of contours, T1s, and metabolite maps that were inputted by the user. C shows the difference of the two Cho/NAA maps for the same axial slice shown in A and B. D shows a 3D overlay of the two contours (pre-RT shown in yellow, mid-RT shown in blue), which can be interacted with when the 3D visualization code is run.

2.7. Statistical Analysis

To determine if any of the previously described overlap statistics can be used as biomarkers of survival, we analyzed each one using Kaplan-Meier curves for OS and PFS [34,35]. For each biomarker of interest, the patient population is first stratified by the median biomarker value, resulting in two equal sized subgroups. Kaplan-Meier curves for OS and PFS are generated for each subgroup, and a log-rank test is used to test for the difference between the survival distributions of the two subgroups [36]. A significant p-value indicates the overlap statistic being used can be considered a significant biomarker of survival [34,35].

Excluding information about spatial volume change, OS and PFS Kaplan-Meier curves are also generated for subjects with Cho/NAA ≥ 2x volume growth and reduction. Percentage of volume change can be tested as an additional biomarker with OS and PFS Kaplan-Meier curves stratified by median volume change.

For an additional assessment of survival, the standard model of Cox Proportional Hazard Regression was used. In order to account for the possible effect of age, ethnicity, MGMT status, and sex on survival, a multivariate analysis to estimate hazard ratios was performed. After measuring the effects of these variables on OS and PFS, only the variables that had significant p-values were included in the final model as parameters to assess the effect of each biomarker on OS and PFS.

2.8. Combined Biomarkers

The combination of two biomarkers may result in the identification of a more robust biomarker of survival. Each spatial overlap statistic can be combined (multiplied) with the direction of volume change (increase or decrease in volume) and the actual percentage change in volume. These combinations of biomarkers can also be evaluated with Kaplan-Meier curves, log-rank tests, and Cox Proportional Hazard regression to be identified as possible biomarkers of survival.

3. Results

3.1. Spatial Overlap

Between the pre- and mid-RT Cho/NAA ≥ 2x volumes of all 27 patients, the median total overlap was 0.796 (range: 0 – 0.964), median Jaccard coefficient was 0.224 (0 – 0.723), median Dice coefficient was 0.365 (0 – 0.839), median volume similarity was -0.142 (-1.54 – 1.77), and median Hausdorff distance was 20.8 mm (8.54 – 92.2 mm).

Statistical analysis between pre- and mid-RT Cho/NAA ≥ 2x volumes showed notable volumetric/spatial changes in several cases. One such case is shown in Figure 2. Although the difference in volumes was very small (0.85 cc, -2% change indicating a slight decrease in volume after two weeks of RT), the total overlap between the two contours was only 57.7%. The difference map in Figure 2C depicts regions of positive change in blue (improvement in Cho/NAA values) and negative change in red (new or

worsening areas of Cho/NAA abnormality). Another case is depicted in Figure 4, where the pre-RT scan Cho/NAA ≥ 2x contour volume was 1.00 cc, and after two weeks of treatment, this volume had grown to 4.96 cc. These volumes had a 51.6% overlap, Jaccard coefficient of 0.063, Dice coefficient of 0.118, volume similarity of -1.54, and Hausdorff distance of 13.7 mm.

3.2. Survival Analysis: Kaplan-Meier curves

Figures 3A and 3B shows Kaplan-Meier curves of OS and PFS with the Dice coefficient as a biomarker. In Figure 3A, 27 patients were stratified by those with a Dice coefficient below and above the median (0.37) and Kaplan-Meier curves of OS were generated for each subgroup. The curves shown in 3A have minimal cross-over and large separation between them, indicating that the Dice coefficient may be a good biomarker of OS. This is further supported by the p-value trending towards significance ($p=0.060$) calculated by a log-rank test. Similarly in Figure 3B, 27 patients were stratified by those with a Dice coefficient below and above the median (0.37) and Kaplan-Meier curves of PFS were generated for each subgroup. With no cross-over and large separation between the curves, it was found that patients with lower Dice coefficient had a higher PFS that was of statistical significance ($p=0.045$). The same result and p-value were observed for the Kaplan-Meier plots for patients stratified by median Jaccard coefficient, shown in Figures 3C and 3D, since stratifying by median resulted in the same subgroups for both Dice and Jaccard coefficients.

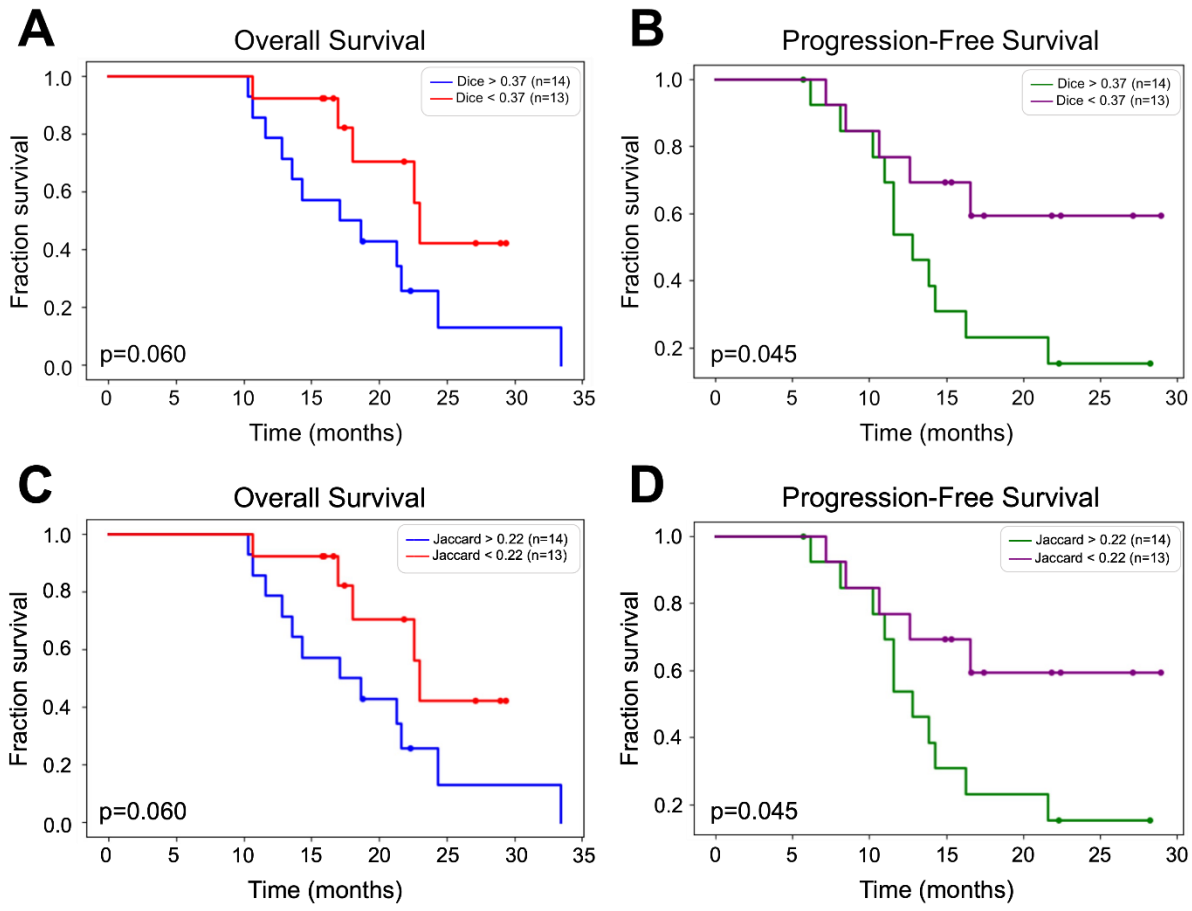

Figure 3. (**A**) Kaplan-Meier curves showing OS stratified by median Dice coefficient. Patients with a higher Dice coefficient had a lower OS. The separation between the curves was determined to be not significant by a log-rank test; however, the results trend towards significance (p=0.060) and may be proven to be significant by a larger cohort. (**B**) Kaplan-Meier curves showing PFS stratified by median Dice coefficient. Patients with a higher Dice coefficient had a lower PFS. The separation between the curves was determined to be significant by a log-rank test (p=0.045). (**C**) Same as (**A**) but instead stratifying OS Kaplan-Meier curves by median Jaccard coefficient. (**D**) Same as (**B**) but instead stratifying OS Kaplan-Meier curves by median Jaccard coefficient.

We also assessed combinations of biomarkers with OS and PFS Kaplan-Meier curves. Total overlap, Dice coefficient and Jaccard coefficient were each combined with 1) direction of volume changed and 2) percentage of volume change. Out of the 27 patients, 13 experienced an increase in Cho/NAA ≥ 2x volume, and 14 experienced a decrease in Cho/NAA ≥ 2x volume after completing two weeks of RT. When analyzed as potential biomarkers of survival, incorporating directionality resulted in no statistically significant difference between groups.

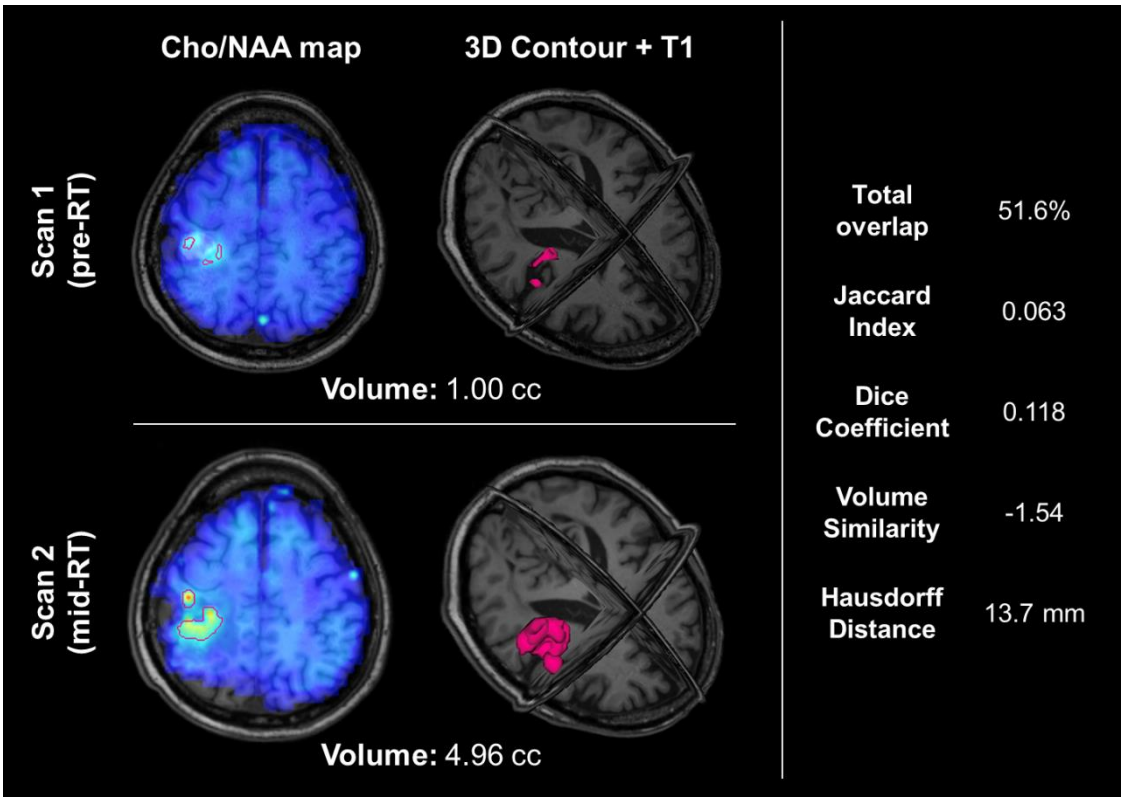

Figure 4. An example of a patient whose Cho/NAA ≥ 2x contour volume increased by almost 400%. The top row shows their pre-RT Cho/NAA ≥ 2x contour and Cho/NAA map overlaid on the T1, as well as a 3D visualization of the Cho/NAA ≥ 2x contour. The bottom row shows their mid-RT contour, Cho/NAA map, and T1. The right-hand side

shows the overlap statistics calculated for the two contours displayed. This patient did not have an IDH mutation and was not MGMT promoter hypermethylated, and experienced progression 8.3 months after resection.

3.3 Survival Analysis: Cox Proportional Hazard Regression

Among the variables sex, race, age at the time of enrollment, and MGMT status, coupled with Jaccard coefficient or Dice coefficient, only race had a significant effect on survival. Patients that were Hispanic or Latino had an increased hazard ratio of 5.08 on PFS (p=0.02) and 7.61 on OS (p=0.01), meaning that being Hispanic or Latino was associated with a lower survival rate.

PFS			**OS**		
Variable	**Hazard ratio**	***p* value**	**Variable**	**Hazard ratio**	***p* value**
Sex	0.62	0.63	Sex	1.34	0.59
Race	5.08	0.02	Race	7.61	0.01
Age	0.97	0.34	Age	0.96	0.14
MGMT status	0.88	0.92	MGMT status	0.35	0.20
Jaccard	2.82	0.61	Jaccard	3.51	0.55
Dice	2.72	0.54	Dice	3.36	0.46

Figure 5. Results of multivariable Cox Proportional Hazard regression. The Hazard ratios measure the multiplicative change of hazard with time associated with each variable. The only significant variable was race with p-values of 0.02 and 0.01 for PFS

and OS, respectively. Being Hispanic or Latino was associated with increased hazard, suggesting lower survival rates.

Therefore, the final model included race as an extraneous variable. Since Jaccard coefficient and Dice coefficient are similar measures of spatial overlap, the final models were 1) Jaccard coefficient and race as parameters and 2) Dice coefficient and race as parameters of multivariate regression to assess the survival rates measured by OS and PFS.

However, with race taken into account, both Dice coefficient and Jaccard coefficient did not have significant effects on PFS or OS.

PFS					
Variable	**Hazard ratio**	***p* value**	**Variable**	**Hazard ratio**	***p* value**
Race	5.04	0.01	Race	4.88	0.01
Jaccard	2.15	0.58	Dice	2.39	0.47
OS					
Sex	5.04	0.01	Sex	4.96	0.01
Jaccard	1.41	0.79	Dice	1.63	0.66

Figure 6. Results of the final model of Cox Proportional Hazard regression. Total of 4 models were generated: 1) Jaccard coefficient and race as parameters to model hazard ratios with PFS 2) Dice coefficient and race as parameters to model hazard ratios with PFS 3) Jaccard coefficient and race as parameters to model hazard ratios with OS 4) Dice coefficient and race as parameters to model hazard ratios with OS. Dice or Jaccard

coefficients were not statistically significant biomarkers of survival with race taken into account ($p>0.05$).

4. Discussion

4.1. Significance of overlap statistics

In this paper, we have used data from a recently completed study that used spectroscopic MRI to guide dose-escalated RT to assess the degree of treatment-induced metabolic changes in the early stages of therapy and investigate how these changes are related to survival outcomes. We use spatial overlap statistics including total overlap, Jaccard coefficient, Dice coefficient, volume similarity, and Hausdorff distance to quantify how the regions of abnormal metabolic activity change after two weeks of treatment. We then used these metrics to identify a relationship between the degree of change in abnormal metabolic activity and survival in the context of motivating the use of adaptive RT planning.

Out of the five different spatial overlap statistics we calculated and tested as biomarkers of survival, the only statistically significant relationships were between Dice coefficient and PFS ($p=0.045$) and between Jaccard coefficient and PFS ($p=0.045$). This p-value is likely attributed to the early separation of curves (around 6 months), no cross-over, and large separation beginning around 11 months. As shown in Figure 3B and 3C, a Dice coefficient of more than 0.37 or a Jaccard coefficient of more than 0.22 was associated with a shorter PFS (median of 18.0 months). This suggests that identifying

tumors that changed more serves as a surrogate for early response to radiation therapy. While the relationships between Dice and Jaccard coefficients and OS (p=0.060 for both) were not statistically significant, they trended towards significance. Although there is separation between the OS curves for the Dice coefficient (Figure 3A) and Jaccard coefficient (Figure 3C), the slight cross-over of curves likely resulted in an insignificant p-value.

However, race was an extraneous variable in that patients that are Hispanic or Latin had a lower survival rate (p=0.01). Therefore, a multivariate analysis was necessary. Combining the effect of races with the possible effects of Dice coefficient and Jaccard coefficient as biomarkers in Cox Proportional Hazard regression model, neither Dice nor Jaccard coefficient had a statistically significant effect on survival.

We believe that a larger cohort is necessary to further investigate this relationship. Kaplan-Meier curves of the patient cohort stratified by all other overlap measures and Cox Proportional Hazards Regression resulted in larger, insignificant p-values. Additionally, combining direction of volume change (increase or decrease of volume) as well as degree of volume change (percentage) with total overlap, Dice coefficient and Jaccard coefficient did not result in the identification of statistically significant biomarkers, likely due to the small sample size.

The patient shown in Figure 4 experienced a nearly 400% increase in metabolic abnormality volume, indicating that this patient's tumor was likely resistant to RT. This is further supported by a relatively short PFS of 8.3 months and lack of positive

prognostic molecular data; this patient did not have an IDH mutation or MGMT promoter hypermethylation [8,37].

Patients with a decrease in Cho/NAA ≥ 2x volume could potentially have the size of their RT treatment field decreased in later treatment. Patients with an increase in Cho/NAA ≥ 2 volume could have their treatment altered, either with a larger/different treatment field or with experimental therapies such as new chemotherapy. While this result suggests evidence of newly proliferating tumor that goes untreated with the original RT plan, it also emphasizes the potential value of a spatial volume overlap analysis tool for providing more insight into volumetric comparisons and show changes due to treatment both quantitatively and visually. This pipeline can be used with other MRI modalities and volumes such as T1w-CE, FLAIR, and DWI. It can also be used with longitudinal data, providing statistical volume comparisons for more than two studies.

4.2. Limitations

Limitations of this study include a small cohort and varying spectroscopic MRI quality. Since the same quality map had to be applied to both scans, by definition, some voxels will be lost, affecting the spatial overlap statistics and all statistical analyses. We are currently in the process of developing new shim-RF head coils that aim to overcome the issue of B0 field inhomogeneity in order to provide improved brain coverage and spectral quality [38]. With only 27 patients, we saw certain trends toward significance, and we believe that a larger study would enable us to investigate these trends more.

5. Conclusions and Further Direction

The analysis technique developed and demonstrated in this report can identify volumetric changes in the volume of metabolic abnormality during early stages of RT and relate these changes to survival outcomes. This pipeline can be applied to a variety of modalities such as performing longitudinal voxel level analysis of recurrence patterns. In this report we demonstrate this technique with spectroscopic MRI data collected for 27 patients pre-RT and after two weeks of RT to assess the utility of adaptive RT planning. Adaptive RT planning could potentially limit irradiation of healthy tissue over the course of RT, however; for this dataset we determined that larger volumetric change indicated response to RT rather than evidence that adaptive RT planning could be useful.

Institutional Review Board Statement: The study was conducted according to the guidelines of the Declaration of Helsinki and approved by the Institutional Review Board (or Ethics Committee) of Emory University (IRB00094188 on 4/14/2017).

Informed Consent Statement: Informed consent was obtained from all subjects involved in the study.

References

1. Gilbert, M.R.; Dignam, J.J.; Armstrong, T.S.; Wefel, J.S.; Blumenthal, D.T.; Vogelbaum, M.A.; Colman, H.; Chakravarti, A.; Pugh, S.; Won, M.; et al. A Randomized Trial of Bevacizumab for Newly Diagnosed Glioblastoma. *New England Journal of Medicine* **2014**, *370*, 699-708, doi:10.1056/nejmoa1308573.
2. Stupp, R.; Mason, W.P.; Van Den Bent, M.J.; Weller, M.; Fisher, B.; Taphoorn, M.J.B.; Belanger, K.; Brandes, A.A.; Marosi, C.; Bogdahn, U.; et al. Radiotherapy plus Concomitant and Adjuvant Temozolomide for Glioblastoma. *New England Journal of Medicine* **2005**, *352*, 987-996, doi:10.1056/nejmoa043330.
3. Stupp, R.; Taillibert, S.; Kanner, A.A.; Kesari, S.; Steinberg, D.M.; Toms, S.A.; Taylor, L.P.; Lieberman, F.; Silvani, A.; Fink, K.L.; et al. Maintenance Therapy With Tumor-Treating Fields Plus Temozolomide vs Temozolomide Alone for Glioblastoma: A Randomized Clinical Trial. *JAMA* **2015**, *314*, 2535-2543, doi:10.1001/jama.2015.16669.
4. Bell, J.B.; Jin, W.; Goryawala, M.Z.; Azzam, G.A.; Abramowitz, M.C.; Diwanji, T.; Ivan, M.E.; del Pilar Guillermo Prieto Eibl, M.; de la Fuente, M.I.; Mellon, E.A. Delineation of recurrent glioblastoma by whole brain spectroscopic magnetic resonance imaging. *Radiation Oncology* **2023**, *18*, 37, doi:10.1186/s13014-023-02219-2.
5. Pope, W.B.; Young, J.R.; Ellingson, B.M. Advances in MRI assessment of gliomas and response to anti-VEGF therapy. *Curr Neurol Neurosci Rep* **2011**, *11*, 336-344, doi:10.1007/s11910-011-0179-x.

6. Tsuchiya, K.; Mizutani, Y.; Hachiya, J. Preliminary evaluation of fluid-attenuated inversion-recovery MR in the diagnosis of intracranial tumors. *AJNR Am J Neuroradiol* **1996**, *17*, 1081-1086.
7. Stupp, R.; Hegi, M.E.; Mason, W.P.; van den Bent, M.J.; Taphoorn, M.J.; Janzer, R.C.; Ludwin, S.K.; Allgeier, A.; Fisher, B.; Belanger, K.; et al. Effects of radiotherapy with concomitant and adjuvant temozolomide versus radiotherapy alone on survival in glioblastoma in a randomised phase III study: 5-year analysis of the EORTC-NCIC trial. *Lancet Oncol* **2009**, *10*, 459-466, doi:10.1016/S1470-2045(09)70025-7.
8. Goryawala, M.; Saraf-Lavi, E.; Nagornaya, N.; Heros, D.; Komotar, R.; Maudsley, A.A. The association between whole-brain MR spectroscopy and IDH mutation status in gliomas. *Journal of Neuroimaging* **2020**, *30*, 58-64, doi:10.1111/jon.12685.
9. Goryawala, M.Z.; Sheriff, S.; Maudsley, A.A. Regional distributions of brain glutamate and glutamine in normal subjects. *NMR in Biomedicine* **2016**, *29*, 1108-1116, doi:10.1002/nbm.3575.
10. Goryawala, M.Z.; Sheriff, S.; Stoyanova, R.; Maudsley, A.A. Spectral decomposition for resolving partial volume effects in MRSI. *Magnetic Resonance in Medicine* **2018**, *79*, 2886-2895, doi:10.1002/mrm.26991.
11. Sabati, M.; Sheriff, S.; Gu, M.; Wei, J.; Zhu, H.; Barker, P.B.; Spielman, D.M.; Alger, J.R.; Maudsley, A.A. Multivendor implementation and comparison of volumetric whole-brain echo-planar MR spectroscopic imaging. *Magnetic Resonance in Medicine* **2015**, *74*, 1209-1220, doi:10.1002/mrm.25510.
12. Cordova, J.S.; Shu, H.K.; Liang, Z.; Gurbani, S.S.; Cooper, L.A.; Holder, C.A.; Olson, J.J.; Kairdolf, B.; Schreibmann, E.; Neill, S.G.; et al. Whole-brain spectroscopic MRI

biomarkers identify infiltrating margins in glioblastoma patients. *Neuro Oncol* **2016**, *18*, 1180-1189, doi:10.1093/neuonc/now036.

13. Brock, K.K. Adaptive Radiotherapy: Moving Into the Future. *Semin Radiat Oncol* **2019**, *29*, 181-184, doi:10.1016/j.semradonc.2019.02.011.
14. Dajani, S.; Hill, V.B.; Kalapurakal, J.A.; Horbinski, C.M.; Nesbit, E.G.; Sachdev, S.; Yalamanchili, A.; Thomas, T.O. Imaging of GBM in the Age of Molecular Markers and MRI Guided Adaptive Radiation Therapy. *J Clin Med* **2022**, *11*, doi:10.3390/jcm11195961.
15. Kim, T.G.; Lim, D.H. Interfractional variation of radiation target and adaptive radiotherapy for totally resected glioblastoma. *J Korean Med Sci* **2013**, *28*, 1233-1237, doi:10.3346/jkms.2013.28.8.1233.
16. Guevara, B.; Cullison, K.; Maziero, D.; Azzam, G.A.; De La Fuente, M.I.; Brown, K.; Valderrama, A.; Meshman, J.; Breto, A.; Ford, J.C. Simulated Adaptive Radiotherapy for Shrinking Glioblastoma Resection Cavities on a Hybrid MRI–Linear Accelerator. *Cancers* **2023**, *15*, 1555, doi:10.3390/cancers15051555.
17. Tseng, C.-L.; Chen, H.; Stewart, J.; Lau, A.Z.; Chan, R.W.; Lawrence, L.S.; Myrehaug, S.; Soliman, H.; Detsky, J.; Lim-Fat, M.J. High grade glioma radiation therapy on a high field 1.5 Tesla MR-Linac-workflow and initial experience with daily adapt-to-position (ATP) MR guidance: A first report. *Frontiers in Oncology* **2022**, *12*, doi:10.3389/fonc.2022.1060098.
18. Schroeder, W.; Martin, K.M.; Lorensen, W.E. *The visualization toolkit an object-oriented approach to 3D graphics*; Prentice-Hall, Inc.: 1998.

19. Lowekamp, B.; Chen, D.; Ibanez, L.; Blezek, D. The Design of SimpleITK. *Frontiers in Neuroinformatics* **2013**, *7*, doi:10.3389/fninf.2013.00045.
20. Mason, D. SU-E-T-33: Pydicom: An Open Source DICOM Library. *Medical physics* **2011**, *38*, 3493-3493, doi:doi.org/10.1118/1.3611983.
21. Davidson-Pilon, C. lifelines: survival analysis in Python. *Journal of Open Source Software* **2019**, *4*, 1317.
22. Ramesh, K.; Mellon, E.A.; Gurbani, S.S.; Weinberg, B.D.; Schreibmann, E.; Sheriff, S.A.; Goryawala, M.; de le Fuente, M.; Eaton, B.R.; Zhong, J.; et al. A multi-institutional pilot clinical trial of spectroscopic MRI-guided radiation dose escalation for newly diagnosed glioblastoma. *Neurooncol Adv* **2022**, *4*, vdac006, doi:10.1093/noajnl/vdac006.
23. Louis, D.N.; Perry, A.; Wesseling, P.; Brat, D.J.; Cree, I.A.; Figarella-Branger, D.; Hawkins, C.; Ng, H.; Pfister, S.M.; Reifenberger, G. The 2021 WHO classification of tumors of the central nervous system: a summary. Neuro-oncology 2021, 23, 1231-1251, doi:10.1093/neuonc/noab106.
24. Gurbani, S.; Weinberg, B.; Cooper, L.; Mellon, E.; Schreibmann, E.; Sheriff, S.; Maudsley, A.; Goryawala, M.; Shu, H.K.; Shim, H. The Brain Imaging Collaboration Suite (BrICS): A Cloud Platform for Integrating Whole-Brain Spectroscopic MRI into the Radiation Therapy Planning Workflow. *Tomography* **2019**, *5*, 184-191, doi:10.18383/j.tom.2018.00028.
25. Ramesh, K.K.; Huang, V.; Rosenthal, J.; Mellon, E.A.; Goryawala, M.; Barker, P.B.; Gurbani, S.S.; Trivedi, A.G.; Giuffrida, A.S.; Schreibmann, E. A Novel Approach to Determining Tumor Progression Using a Three-Site Pilot Clinical Trial of

Spectroscopic MRI-Guided Radiation Dose Escalation in Glioblastoma. *Tomography* **2023**, *9*, 362-374, doi:10.3390/tomography9010029.

26. Gurbani, S.S.; Schreibmann, E.; Maudsley, A.A.; Cordova, J.S.; Soher, B.J.; Poptani, H.; Verma, G.; Barker, P.B.; Shim, H.; Cooper, L.A.D. A convolutional neural network to filter artifacts in spectroscopic MRI. *Magn Reson Med* **2018**, *80*, 1765-1775, doi:10.1002/mrm.27166.
27. Maudsley, A.A.; Darkazanli, A.; Alger, J.R.; Hall, L.O.; Schuff, N.; Studholme, C.; Yu, Y.; Ebel, A.; Frew, A.; Goldgof, D.; et al. Comprehensive processing, display and analysis for in vivo MR spectroscopic imaging. *NMR Biomed* **2006**, *19*, 492-503, doi:10.1002/nbm.1025.
28. Maudsley, A.A.; Domenig, C.; Govind, V.; Darkazanli, A.; Studholme, C.; Arheart, K.; Bloomer, C. Mapping of brain metabolite distributions by volumetric proton MR spectroscopic imaging (MRSI). *Magn Reson Med* **2009**, *61*, 548-559, doi:10.1002/mrm.21875.
29. Maudsley, A.A.; Domenig, C.; Sheriff, S. Reproducibility of serial whole-brain MR spectroscopic imaging. *NMR Biomed* **2010**, *23*, 251-256, doi:10.1002/nbm.1445.
30. Veenith, T.V.; Mada, M.; Carter, E.; Grossac, J.; Newcombe, V.; Outtrim, J.; Lupson, V.; Nallapareddy, S.; Williams, G.B.; Sheriff, S.; et al. Comparison of inter subject variability and reproducibility of whole brain proton spectroscopy. *PLoS ONE* **2014**, *9*, e115304, doi:10.1371/journal.pone.0115304.
31. Zhang, Y.; Taub, E.; Salibi, N.; Uswatte, G.; Maudsley, A.A.; Sheriff, S.; Womble, B.; Mark, V.W.; Knight, D.C. Comparison of reproducibility of single voxel spectroscopy

and whole-brain magnetic resonance spectroscopy imaging at 3T. *NMR Biomed* **2018**, *31*, e3898, doi:10.1002/nbm.3898.

32. Tustison, N.J.; Gee, J.C. Introducing Dice, Jaccard, and other label overlap measures to ITK. *Insight J* **2009**, *2*, 707.
33. Huttenlocher, D.P.; Klanderman, G.A.; Rucklidge, W.J. Comparing images using the Hausdorff distance. *IEEE Transactions on pattern analysis and machine intelligence* **1993**, *15*, 850-863, doi:10.1109/34.232073.
34. Bland, J.M.; Altman, D.G. Statistics Notes: Survival probabilities (the Kaplan-Meier method). *BMJ* **1998**, *317*, 1572-1580, doi:10.1136/bmj.317.7172.1572.
35. Bland, J.M.; Altman, D.G. Survival probabilities (the Kaplan-Meier method). *BMJ* **1998**, *317*, 1572, doi:10.1136/bmj.317.7172.1572.
36. Bland, J.M.; Altman, D.G. The logrank test. *BMJ* **2004**, *328*, 1073, doi:10.1136/bmj.328.7447.1073.
37. Binabaj, M.M.; Bahrami, A.; ShahidSales, S.; Joodi, M.; Joudi Mashhad, M.; Hassanian, S.M.; Anvari, K.; Avan, A. The prognostic value of MGMT promoter methylation in glioblastoma: a meta-analysis of clinical trials. *Journal of Cellular Physiology* **2018**, *233*, 378-386, doi:10.1002/jcp.25896.
38. Han, H.; Song, A.W.; Truong, T.K. Integrated parallel reception, excitation, and shimming (iPRES). *Magnetic Resonance in Medicine* **2013**, *70*, 241-247, doi:10.1002/mrm.24766/